EFDA–JET–CP(14)01/28

C. Reux, V. Plyusnin, B. Alper, D. Alves, B. Bazylev, E. Belonohy, S. Brezinsek, J. Decker, S. Devaux, P. de Vries, A. Fil, S. Gerasimov, I. Lupelli, S. Jachmich, E.M. Khilkevitch, V. Kiptily, R. Koslowski, U. Kruezi, M. Lehnen, A. Manzanares, J. Mlynář, E. Nardon, E. Nilsson, V. Riccardo, F. Saint-Laurent, A.E. Shevelev, C. Sozzi and JET EFDA contributors

Runaway Beam Studies During Disruptions at JET-ILW

Runaway Beam Studies During Disruptions at JET-ILW

C. Reux[1], V. Plyusnin[2], B. Alper[3], D. Alves[2], B. Bazylev[4], E. Belonohy[5], S. Brezinsek[7], J. Decker[1], S. Devaux[5], P. de Vries[8], A. Fil[1], S. Gerasimov[3], I. Lupelli[3], S. Jachmich[5,6], E.M. Khilkevitch[12], V. Kiptily[3], R. Koslowski[7], U. Kruezi[3], M. Lehnen[8], A. Manzanares[10], J. Mlynář[9], E. Nardon[1], E. Nilsson[1], V. Riccardo[3], F. Saint-Laurent[1], A.E. Shevelev[12], C. Sozzi[11]
and JET EFDA contributors*

JET-EFDA, Culham Science Centre, OX14 3DB, Abingdon, UK

[1]CEA, IRFM, F-13108 Saint-Paul-lez-Durance, France
[2]Instituto de Plasmas e Fuso Nuclear, Instituto Superior Tcnico, Universidade de Lisboa, Lisboa, Portugal
[3]CCFE, Culham Science Centre, Abingdon OX14 3DB, UK
[4]Institut fr Hochleistungsimpuls und Mikrowellentechnik, Karlsruhe Institute of Technology, Campus Nord,76021 Karlsruhe, Germany
[5]EFDA-CSU, Culham Science Centre, Abingdon OX14 3DB, UK
[6]Laboratoire de Physique des Plasmas-Laboratorium voor Plasmafysica, Association EURATOM-Belgian State Institute ERM/KMS, B-1000 Brussels, Belgium
[7]Forschungszentrum Jlich GmbH, Institut fr Energie-und Klimaforschung-Plasmaphysik, 52425 Jlich, Germany
[8]ITER Organization, Route de Vinon sur Verdon, 13115 St Paul Lez Durance, France
[9]Institute of Plasma Physics AS CR, Za Slovankou 3, 18200 Prague 8, CZ
[10]Association Euratom-CIEMAT, Moncloa, Avd. Complutense, 22, 28040 Madrid 3, Spain
[11]Istituto di Fisica del Plasma CNR-EURATOM, via Cozzi 53, 20125 Milano, Italy
[12]Ioffe Physical-Technical Institute of the Russian Academy of Sciences, Polytechnicheskaya 26, St Petersburg, 194021, Russia
** See annex of F. Romanelli et al, "Overview of JET Results", (24th IAEA Fusion Energy Conference, San Diego, USA (2012)).*

Preprint of Paper to be submitted for publication in Proceedings of the
21st International Conference on Plasma Surface Interactions, Kanazawa, Japan
26th May 2014 - 30th May 2014

ABSTRACT

Runaway electrons (RE) during disruptions are a concern for future tokamaks including ITER with its metallic wall. Experiments with the JET ITER-like Wall (JET-ILW) showed that RE were very rare in spontaneous disruptions, unlike with the carbon-wall (JET-C). However, RE beams up to 380kA were obtained using massive injection (MGI) of argon in JET-ILW divertor discharges. Although the runaway domain entry points are unchanged, higher RE currents have been obtained inside the JET-ILW MGI-generated RE domain when compared to JET-C. This might be due to the influence of the metallic wall on the current quench plasma. Temperatures of 900°C have been observed following RE impacts on beryllium tiles. Heat deposition depth of 1 to 2mm has to be assumed to match the tile cooling time. 3D simulations of the RE energy deposition and diffusion using the ENDEP/MEMOS codes show that material melting is unlikely with 100kA RE beams.

1. INTRODUCTION

Runaway Electrons (RE) during disruptions are one of the major concerns for ITER and future tokamaks. Several MA of multi-MeV RE may be expected in ITER, with risks of damage to the plasma facing components (PFC) and significant impact on operations if repairs are needed. JET in its ITER-like wall configuration (tungsten, beryllium) is most suited to study runaway electrons in the closest conditions to ITER. The influence of a metal wall on RE generation and behaviour can thus be investigated. The impact of a RE beam on metallic plasma facing components can also be studied. This is important as this type of wall material is more sensitive to transient heat loads than carbon wall. Cross-comparisons with similar experiments in carbon-wall can be made. This article is divided as follows. The first part presents the experimental background and conditions. The second part is devoted to the analysis of the influence of the metallic wall on the RE generation and behaviour during the disruption. The third part is focused on the observations and simulations of runaway electrons impact on plasma facing components.

2. EXPERIMENTAL BACKGROUND

Runaway electrons during spontaneous disruptions were observed on a regular basis with JET Carbon wall (JET-C)[1]. On the contrary, spontaneous disruptions with JET ITER-like wall (JET-ILW) tend to produce almost no runaway electrons [2, 3]. During the whole course of the first JET-ILW campaigns (more than 4000 plasma pulses) only two RE beams during disruptions were observed and in very peculiar conditions (disruption during ramp-up at low density due to control failure [4]). A couple other non-disruptive pulses with low-energy runaway electrons during plasma current ramp-up have also been observed. Even intentional disruptions designed to generate runaways electrons were found to produce much lower RE currents than their JET-C equivalents [5]. Runaway electron generation is governed by the ratio of an accelerating electric E_a field over a critical field $E_c = \frac{n_e e^3 \ln \Lambda}{4\pi \in_0^2 m_e c^2}$ where n_e is the electron density and $ln\Lambda$ is the coulombian logarithm. The critical field is a relativistic correction to the Dreicer primary generation mechanism [6] and a major

parameter for the avalanche mechanism [7]. Major dependencies of the runaway electron production are thus the accelerating electric field E_a, the electron density n_e, the effective charge Z_{eff} and the background plasma temperature. Other indirect dependencies are the toroidal field B_t, magnetic turbulence [8], initial plasma current I_p and plasma shape (circular plasmas tend to generate more runaway electrons than elongated divertor shapes [9, 10]). Toroidal field in particular has been observed on most of large tokamaks as a major dependency for RE production. The lower amount of RE during spontaneous JET-ILW disruptions is partly due to the slower current quenches [2] but also different radiation characteristics between beryllium and carbon in some specific disruption conditions [5].

The best settings to obtain disruption-generated runaway electrons in JET-C were by using Massive Gas Injection (MGI) of pure Argon using the Disruption Mitigation Valve (DMV). This valve is normally used with a 90% Deuterium + 10% Argon mixture to mitigate spontaneous disruptions during routine operation [11]. Pure argon accelerates the current quench of disruptions [12] hence increasing the accelerating electric field responsible for RE generation. It also keeps a moderate electron density in plasma core due to the low mixing efficiency of argon. On the contrary, decreasing the argon fraction may lead to increased electron density thanks to the better mixing efficiency of deuterium, thus reducing the amount of runaway electrons. Massive Gas Injection of mixtures of deuterium and argon in various fractions f_{Ar} is therefore the best method to generate the widest range of RE currents in a reliable and controlled way. Other control parameters are the initial plasma density and the toroidal field. This allows the determination of the point where RE start to appear, namely the border of the RE/no RE domain in the space defined by (B_t,f_{Ar},n_e). This can be compared with similar pulses in JET-C.

3. EFFECT OF THE ITER-LIKE-WALL ON RUNAWAY ELECTRONS GENERATION

This section is focused on the mapping of the RE operational domain in the previously defined space (B_t,f_{Ar},n_e). The amount of runaways is measured using the deviation of plasma current from an exponential decay during current quench and from the amount of photoneutrons produced by the RE interaction with background gas or solid material. The runaway current measurement has unfortunately large uncertainties due to the fact that the plasma current decay is not purely exponential even without any runaway electron. Measurement of RE currents below 50kA are therefore difficult with this method. The neutron amount is more accurate but cannot be used to compare JET-C and JET-ILW cases directly. The photoneutron generation threshold is indeed different for carbon and beryllium/tungsten. It can still be used to determine the presence/absence of runaway electrons above a certain energy and to compare disruptions with the same wall material.

3.1. BOUNDARY LOCATION

The RE domain boundary location was determined by scans in argon fraction and toroidal field. Figure 1 shows the RE currents obtained with these parameters in a divertor configuration. Increasing

B_t and f_{Ar} increases the RE amount as expected. Up to 380kA of RE current have been obtained with pure argon and B_t = 3.0T . This shows that an all-metal wall does not hinder completely the generation of high RE current.

The location of transitions from the no-RE region to the RE region is not significantly changed between JET-C and JET-ILW: at B_t = 3.0T (I_p = 2.0MA), runaway electrons appear around f_{Ar} = 40%. At f_{Ar} = 100%, runaway electrons appear at B_t = 1.2T (I_p = 1.5MA). In order to interprete these operational parameters in terms of physics values, the accelerating electric field and the critical electric field have to be calculated. The accelerating electric field is computed by a lumped circuit calculation which takes into account mutual inductances between the plasma, poloidal field coils and vessel structures. Figure 2 shows that larger RE currents are correlated with higher accelerating fields, although the toroidal field plays a role as high accelerating fields can produce little amounts of RE if the toroidal field is low enough. The ratio between the accelerating electric field and the critical electric field is also expected to have an impact on the RE production, but is more difficult to estimate during the current quench due to absence of density measurements. The density, which is one of the main parameters in the critical field calculation can indeed only be measured up to the thermal quench or in the end of the current quench. A large part of the current quench is not accessible due to the refraction of the interferometer beam by density gradients. An estimation of the critical field can be done using two different density measurements: the last point before the laser is refracted, usually around the thermal quench, or the first points at the end of the current quench. The last density measurement before the start of the current quench is used to compute the critical field and the E_a/Ec fraction shown on figure 3. The real critical field is expected to be higher as the density usually rises at the beginning of the current quench [13], but this gives an estimate and a lower bound of Ec. Figure 3 clearly shows two domains in the (E_a/E_c, B_t) space. As expected, low E_a/E_c fractions generate RE only at high toroidal fields whereas higher E_a/E_c fractions can generate significant amounts of RE even at low B_t. This shows that the initial density rise is representative of the actual density reached during the phase where RE are created. It also explains why high Argon fractions in the DMV tend to produce high amounts of RE: Argon MGI leads to fast current quenches and hence large electric fields due to its ability to radiate a large amount of energy but has a lower mixing efficiency than deuterium, leading to lower densities during the current quench. The density measured at the end of the current quench can also be used to calculate the critical field. For proper comparison between pulses where the first available measurement does not happen at the same time, the value at 5% of the initial plasma current is taken. The presence of two separate domains is much less clear with this density value than with the pre-TQ density calculation method. This could mean that the presence of a large runaway electron beam itself may have an influence on the post-CQ density.

For most of the JET-ILW runaway electron pulses, RE energies were measured by Hard X-Ray (HXR) spectrometers. RE electrons energies are then deconvoluted from HXR spectrums using the DeGaSum code [14]. It shows that RE beams at higher currents have also higher energy up to

18-20MeV for semi-plateaux RE regimes (380kA and beyond). Mean and maximum HXR energy for a selection of pulses are given on figure 4. Energies are plotted versus the amount of photoneutrons instead of runaway electrons current because some pulses clearly show signs of runaway electrons but the current is too low to be measured. As shown, a higher number of RE (higher currents or higher amount of photoneutrons) is correlated with higher HXR energies and therefore higher RE energies. A deconvoluted spectrum for a 50kA RE beam is given on figure 5 and shows a maximum energy of 20MeV.

3.2. COMPARISON JET-C AND JET-ILW

Although the location of transitions points between RE/no-RE zones is similar between JET-C and JET- ILW, the amount of RE once this boundary is crossed is significantly different for pure argon cases. 5 out of the 6 comparison pulses have higher RE currents in JET-ILW than in JET-C (figure 6). The accelerating electric field (calculated in the same way as presented in section 3.1) is identical between JET-C and JET- ILW cases. Consequently, the difference has to lie on the critical field or on RE loss mechanisms. The initial effective charge Z_{eff} is different between JET-C and JET-ILW due to the wall material. It might explain part of the difference as Z_{eff} is thought to play a role in RE generation [15]. Current quench temperature or magnetic turbulence may also have an impact on the RE generation rate. The only obvious difference observed so far lies in the density at the end of the current quench. Figure 7 shows the line-integrated density as measured by two central chords of the fast infrared interferometer. The initial density rise before the thermal quench is very similar in both JET-ILW and JET-C cases although a small delay is observed in JET-ILW cases. However, the density at the end of the current is higher in JET-C cases at the same fraction of the remaining plasma current. This is a good candidate to explain the larger RE current observed in JET-ILW than in JET-C in massive argon injection disruptions. The fact that the electron density remains higher for a longer time in JET-C cases despite a similar current quench timing tends to show that the processes leading to the density spike during the current quench (plasma recombination, outgassing from the wall) might be different in JET-ILW due to the change in wall material. This also tends to show that in spite of the large amount of gas injected by MGI, it does not completely dominate the late-CQ density processes.

4. RUNAWAY ELECTRON IMPACTS ON PLASMA FACING COMPONENTS

4.1. IMPACT OBSERVATIONS

Most of the plasmas where RE were observed during the disruption were in divertor elongated configuration which is vertically unstable. In this particular configuration, it is found that RE beams move towards the upper dump plate (UDP). The upper dump plate is composed of 64 ribs, which are series of beryllium tiles covering the top part of the chamber poloidally. The dump plate is thus toroidally discrete. RE impact is observed via a wide angle infrared (IR) camera with 20ms time resolution. It takes place at the end of the current quench and is correlated with the final drop of the

current. It is characterized by a series of poloidally localized hots spots (one per dump plate rib). Temperature footprint is roughly gaussian along projections by the camera of poloidal and toroidal directions, with decay lengths 32 ± *8mm* and 10 ± *5mm* respectively. IR picture of the impact is shown on figure 8. The area of RE interaction is comparable with JET-C data [16] although the dump plate geometry was different. Since the camera time step is larger than the duration of the current quench and significantly longer that the estimated duration of the RE impact (about 1ms according to the neutron signal spike), the maximum temperature reached by the tile might be not completely resolved. However, the tile cooling time is well captured. Simple simulations of 1D heat diffusion inside the tile using a finite difference model have been done in order to have a rough estimate of the deposited energy needed to account for the tile cooling time as viewed by the infrared cameras. A simplified 1ms rectangular time step for RE impact is assumed, based on the duration of the final neutron spike which is the signature of RE interaction with the wall at the end of a RE beam. Two fit parameters are varied to try to match the simulated surface temperature: the incident power and the deposition depth. It is indeed very clear that the cooling time decay and a sensible peak surface temperature cannot be matched at the same time while assuming only surface heat deposition. The incident power during the 1ms step determines the total amount of energy deposited into the tile, which is reflected by the temperature observed after several seconds cooling. On the contrary, the deposition depth determines the initial peak temperature and the initial cooling temperature waveform, before the temperature becomes more homogenous inside the tile. Results for Pulse Numbers: 85020 and 85021 are shown on figures 9 and 10. The best fit parameters for Pulse Number: 85020 are $P_{incident} = 3.5 GW.m^{-2}$ deposited over $d_{depth} = 1.4 mm$ depth. One has to bear in mind that the depth has a large uncertainty due to the fact that the deposition is likely not to be homogenous in depth and that the peak temperature might not be resolved by the infrared camera. Cooling waveform for Pulse Number: 85021 is best fitted with an incident power $P_{incident} = 4.1 GW.m^{-2}$ and deposition depth $d_{depth} = 2.5 mm$. The larger total energy deposited is consistent with the fact that the RE current is larger on this pulse (100KA on Pulse Number: 85021 versus 50kA on Pulse Number: 85020). The measured peak temperature is lower on Pulse Number: 85021 as seen on figure 10 but this is likely to be due to the low time resolution of the diagnostic. The cooling time is indeed slightly longer for Pulse Number: 85021, showing that the total deposited energy is higher.

4.2. IMPACT SIMULATIONS

The RE electron impact was simulated using the ENDEP/MEMOS suite of codes [17]. ENDEP is a Monte-Carlo code which computes the volumetric energy deposition inside the material. In a second step, MEMOS computes the temperature distribution in the tile taking into account temperature-dependent properties of beryllium. Incident relativistic electrons gyrate along magnetic field lines, and the ratio between their transverse and parallel energy is assumed to be $E_{tr}/E_{par} = 0.01$. The tile geometry is taken from [18] and leads to a field line angle of 2.7 with the incident surface. The width of the interaction (wetted area) is assumed to be 2mm (6̃mm projected on the tile surface).

Two JET RE impacts (Pulse Numbers: 85020 and 85021) with good infrared data were simulated. Figure 11a shows the energy map deposition for both pulses, normalized to the total incident energy. A significant part of the energy is deposited inside the bulk of the tile: most of it is absorbed in the first 2mm of the tile which is in good agreement with the cooling time analysis from IR data (see previous section 4.1). The exact energy deposition pattern depends on the RE energy spectrum. In both cases though, only 25% of the beam total thermal energy is dissipated in the tile $\left(\frac{Q_{abs}}{Q_{tot}} = 25\%\right)$: part of the RE pass through the tile and escape. Similarly, only 10% of the RE current is lost in the tile: the rest escapes from the upper surface to continue its path along the propagation direction of the RE beam. Consequently, conversion and dissipation of the RE beam magnetic energy is low. The energy spectrum of the escaping electrons is slightly altered by the tile crossing (see figure 12). Although the IR pattern shows that more than one tile is impacted by the beam, multi-tile crossing simulations are not yet implemented in the code.

ENDEP results were then used as inputs for MEMOS simulations. MEMOS is a 3D thermal diffusion code which takes into account temperature-dependent material properties as well as melt motion. As ENDEP only provides energy deposition functions normalized to the total deposited, several heat flux scenarios were tested from $P_{incident} = 10 GW.m^{-2}$ to $P_{incident} = 120 GW.m^{-2}$ with a 1ms rectangular time window for RE interaction with the wall. Simulations results show that the melting threshold is $P = 97 GW.m^{-2}$ for Pulse Number: 85020 and $P = 103 GW.m^{-2}$ for Pulse Number: 85021. Although not directly comparable due to geometry differences and measurements uncertainty, the scenario ($50 GW.m^{-2}$) is qualitatively close to the experimental values (see figure 11b). The discrepancy between the estimated incident power for this case and the simple simulation carried out on previous section is still to be explained, and might be due to the more precise geometry used in ENDEP/MEMOS. The maximum reached temperature is 960 K for Pulse Number: 85020 and 990 K or Pulse Number: 85021. The cooling time during the first 200ms is in qualitative agreement. These results show that it is likely that no melting occurred during these two events (50kA and 100kA RE current), although some melting may be reached for higher RE currents.

5. CONCLUSION AND DISCUSSION

Rrunaway electrons have been observed in a metallic environment at JET. Although RE are rare during spontaneous disruptions, they can still be generated using massive gas injections of argon. Argon dominates the disruption plasma content thus decreasing the effect of the intrinsic impurities (carbon or beryllium) on the current quench dynamics. Therefore, the conditions in which RE appear are similar between JET-C and JET-ILW: high toroidal field, high accelerating electric field and low densities (leading to lower critical electric field for RE generation) favor large RE generation. However, preliminary results on a limited number of pulses tend to show that inside the RE generation space, beams can reach higher currents and be sustained for longer times in JET-ILW than JET-C. This might be due to different density behaviour in late stages of the current quench, where the injected argon no longer dominates the cold plasma content. Outgassing from the wall during this

stage may indeed be different between JET-C and JET-ILW. Lower densities are measured during the latest stages of the current quench in JET-ILW. RE energies were measured up to 20MeV for 200 to 380kA RE beams. RE impacts on beryllium plasma facing components were observed with temperatures up to 900C on the upper dump plate. The impact pattern is distributed along the dump-plate ribs, with approximately 30mm wide poloidal footprint. Cooling time analysis using a 1D heat diffusion model of the impact of 50kA and 100kA beams show that the energy deposition depth is 1 to 2mm inside the tile. More refined simulations using the ENDEP/MEMOS suite of code confirm a 2mm deposition depth. They also show that only 25% of the beam thermal energy and 10% of its current are deposited inside one single tile. 3D heat diffusion calculations tend to show that no melting has occurred for 100kA events, with a maximum temperature corresponding to $50 GW.m^{-2}$ during 1ms.

ACKNOWLEDGMENTS

This work was supported by EURATOM and carried out within the framework of the European Fusion Development Agreement. The views and opinions expressed herein do not necessarily reflect those of the European Commission or the ITER Organization.

REFERENCES

[1]. V. Plyusnin, et al., Latest Progress in Studies of Runaway Electrons in JET Proceedings of the 24th IAEA Fusion Energy Conference (FEC2012), San Diego, USA 8th October 2012 – 13th October 2012.

[2]. P. C. de Vries, et al., The Impact of the ITER-Like Wall at JET on Disruptions, Plasma Physics and Controlled Fusion **54** (12) (2012) 124032.

[3]. M. Lehnen, et al., Impact and Mitigation of Disruptions with the ITER-Like Wall in JET, Nuclear Fusion **53** (9) (2013) 093007.

[4]. V. Riccardo, et al., Operational Impact on the {JET} ITER-Like Wall In-Vessel Components, Fusion Engineering and Design (0) (2014) –.

[5]. G. Papp, et al., The Effect of ITER-Like Wall on Runaway Electron Generation in JET, Nuclear Fusion **53** (12) (2013) 123017.

[6]. J. Connor, R. Hastie, Relativistic Limitations on Runaway Electrons, Nuclear Fusion **15** (3) (1975) 415.

[7]. M. Rosenbluth, S. Putvinski, Theory for Avalanche of Runaway Electrons in Tokamaks, Nuclear Fusion **37** (10) (1997) 1355.

[8]. L. Zeng, et al., Experimental Observation of a Magnetic-Turbulence Threshold for Runaway-Electron Generation in the Textor Tokamak, Physical Review Letters **110** (2013) 235003.

[9]. E. Hollmann, et al., Control and Dissipation of Runaway Electron Beams Created During Rapid Shutdown Experiments in diii-d, Nuclear Fusion **53** (8) (2013) 083004.

[10]. F. Saint-Laurent, C. Reux, J. Bucalossi, A. Loarte, S. Bremond, C. Gil, P. Maget, P. Moreau, J.-L. Sgui, Disruption and Runaways Electron Mitigation Studies on Tore SupraProceedings of the 23rd IAEA Fusion Energy Conference (FEC2010), Daejeon, Korea.

[11]. C. Reux, et al., Use of the Disruption Mitigation Valve in Closed Loop for Routine Protection at {JET}, Fusion Engineering and Design 88 (68) (2013) 1101 – 1104, Proceedings of the 27th Symposium on Fusion Technology (SOFT-27); Lige, Belgium, September 24–28, 2012.

[12]. M. Lehnen, et al., Disruption Mitigation by Massive Gas Injection in JET, Nuclear Fusion **51** (12) (2011) 123010.

[13]. G. Pautasso, et al., Contribution of ASDEX Upgrade to Disruption Studies for ITER, Nuclear Fusion **51** (10) (2011) 103009.

[14]. A. Shevelev, et al., Reconstruction of Distribution Functions of Fast Ions and Runaway Electrons in Fusion Plasmas using Gamma-Ray Spectrometry with Applications to ITER, Nuclear Fusion **53** (12) (2013) 123004.

[15]. Y. Igitkhanov, Generation of Runaway Electrons in Multicomponent JET Boundary Plasmas. This conference, P3-081.

[16]. G. Arnoux, et al., Heat Load Measurements on the {JET} First Wall During Disruptions, Journal of Nuclear Materials **415** (1, Supplement) (2011) S817 – S820, Proceedings of the 19th International Conference on Plasma-Surface Interactions in Controlled Fusion.

[17]. B. Bazylev, et al., Modeling of Runaway Electron Beams for {JET} and {ITER}, Journal of Nuclear Materials **415** (1, Supplement) (2011) S841 – S844, Proceedings of the 19th International Conference on Plasma-Surface Interactions in Controlled Fusion.

[18]. B. Bazylev, et al., Modeling of the Impact of Runaway Electrons on the {ILW} in {JET}, Journal of Nuclear Materials **438**, Supplement (0) (2013) S237 – S240, Proceedings of the 20th International Conference on Plasma-Surface Interactions in Controlled Fusion Devices.

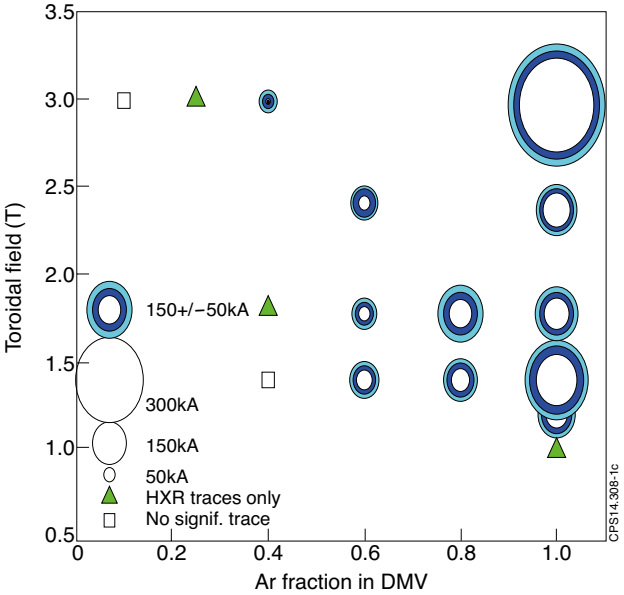

Figure 1: Operational domain for RE production in JET-ILW. Error bars for RE current are given by colored circles.

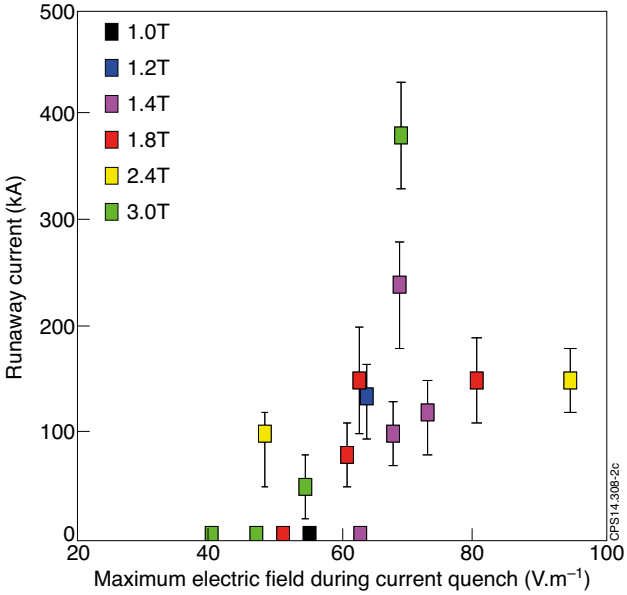

Figure 2: Maximum RE current versus maximum electric field during current quench at various B_t for JET-ILW.

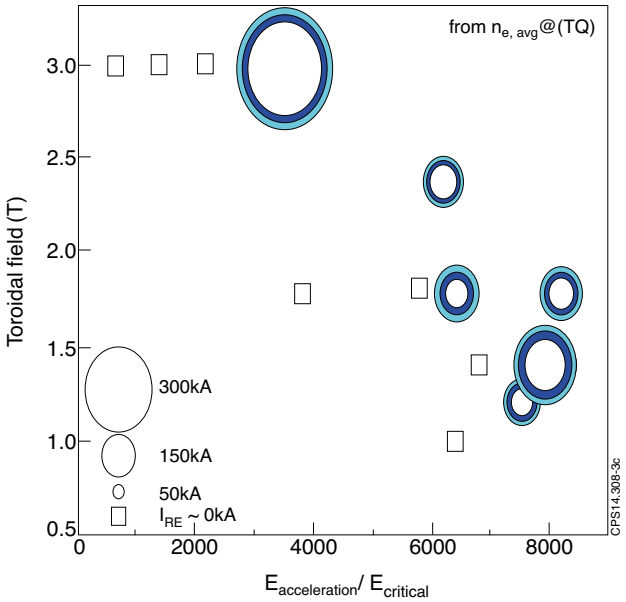

Figure 3: RE current versus toroidal field and ratio of electric field E_a over critical field E_c. Density measurement taken from last valid point at thermal quench.

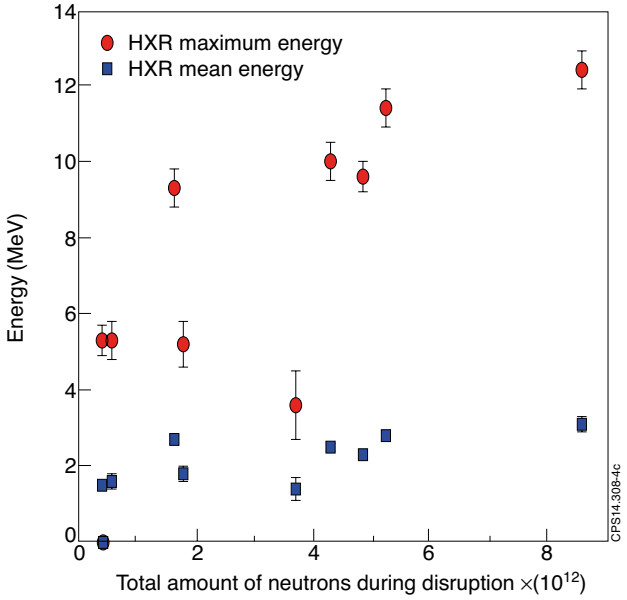

Figure 4: Mean and maximum HXR energy for a selection of RE pulses from 0 to 240kA. Neutrons are used for proxies for RE amounts because of too low RE currents in most of the cases.

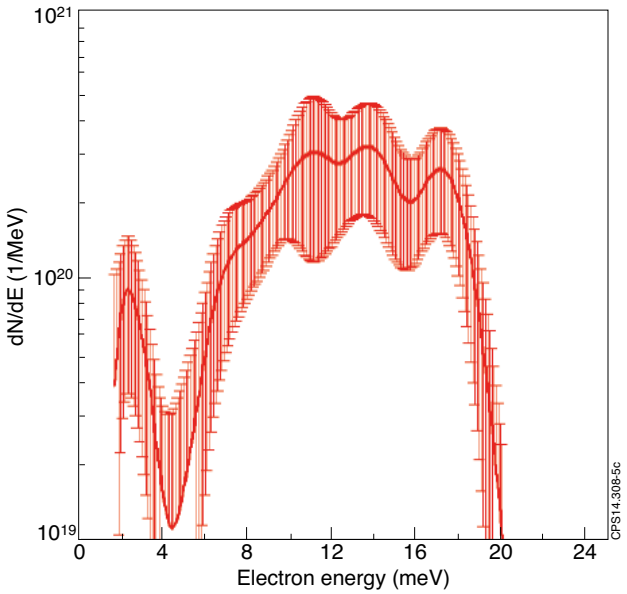

Figure 5: Deconvoluted energy spectrum for a 50kA RE disruption in JET-ILW.

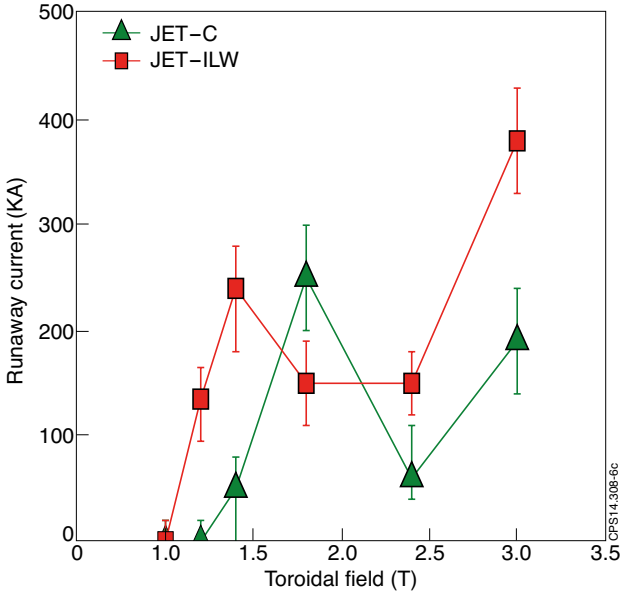

Figure 6: RE currents for similar JET-C and JET-ILW pulses at different B_t values.

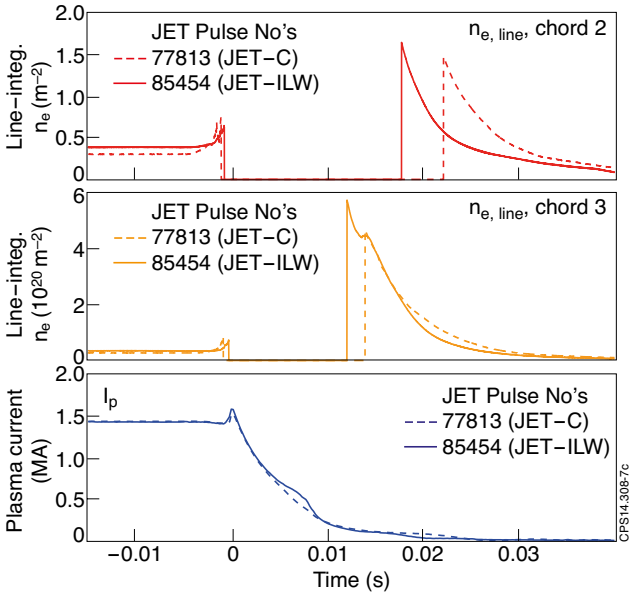

Figure 7: Electron density comparison at thermal quench and at the end of current quench for similar JET-C and JET-ILW disruptions (f_{Ar} = 100%). No significant RE current in JET-C versus 135kA in JET-ILW.

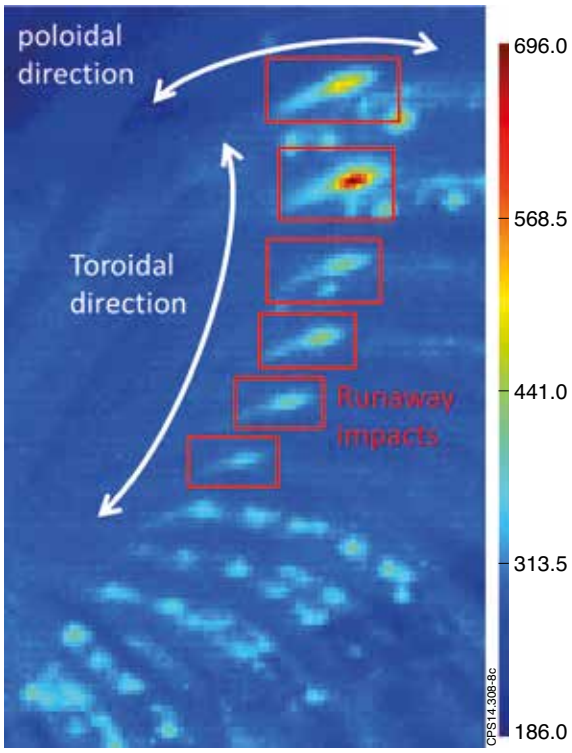

Figure 8: Infrared image of RE beam impact on upper dump plate.

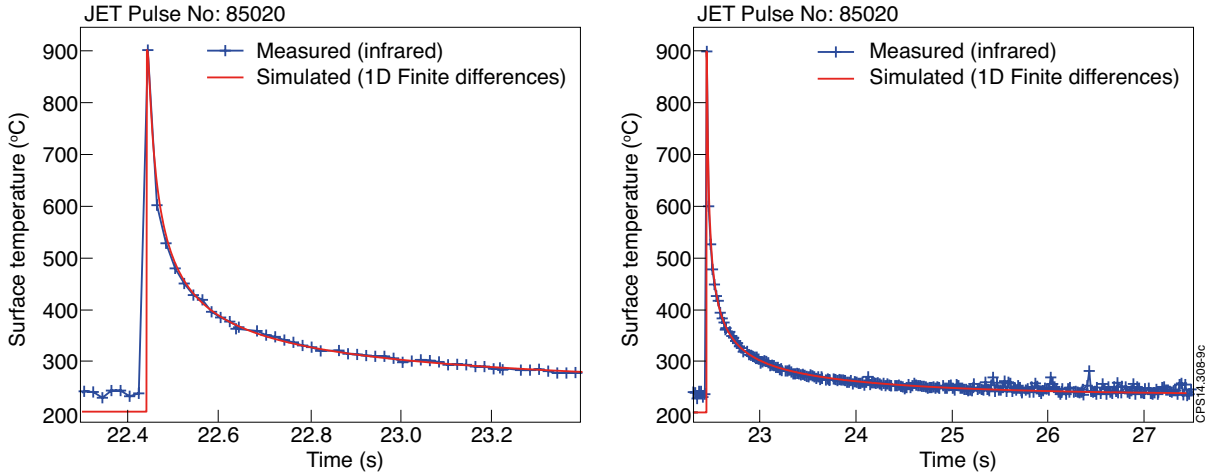

Figure 9: Temperature for Pulse Number: 85020 measured by IR camera and simulated by 1D thermal diffusion (a) closeup on initial temperature rise (b) Cooling phase.

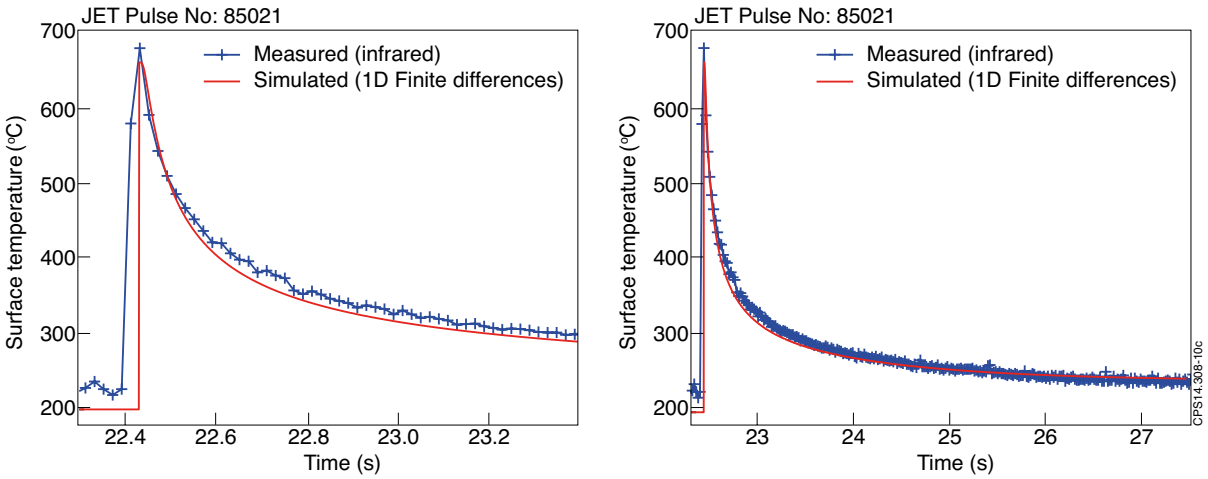

Figure 10: Temperature for Pulse Number: 85021 measured by IR camera and simulated by 1D thermal diffusion (a) closeup on initial temperature rise (b) Cooling phase.

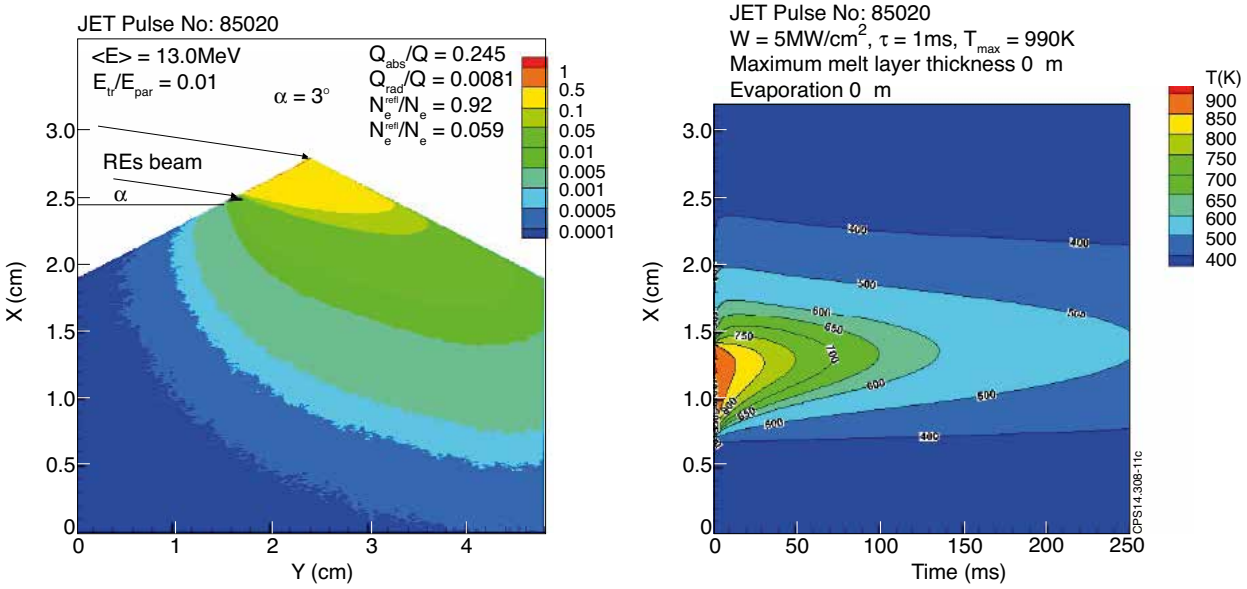

Figure 11: ENDEP/MEMOS: (a) Energy deposition functions for a RE impact on a dump plate tile. (b) Surface temperature along the toroidal direction on a dump plate tile.

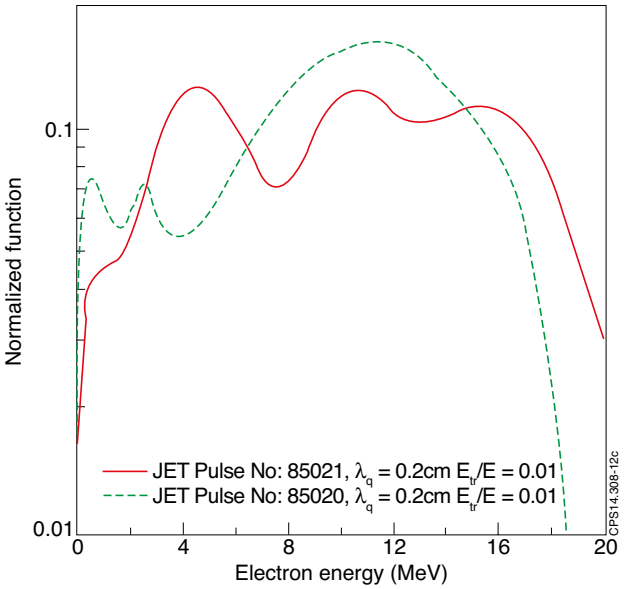

Figure 12: Energy spectrum for escaping electrons (after passing through a dumpplate tile)